SCATTERING BY SMALL THIN DIELECTRIC PARTICLES

D. A. Ksienski* and T.B.A. Senior
Radiation Laboratory
Department of Electrical Engineering and Computer Science
The University of Michigan
Ann Arbor, Michigan 48109

ABSTRACT

In the analysis of electromagnetic scattering by distributions of small dielectric particles an approximation to the scattered field can be obtained by representing the electrical interaction of the particles in terms of the dipole moments of the individual particles. The calculation of the moments necessitates the solution of certain static scattering problems, and this becomes numerically difficult when the particles are thin. An integral equation formulation of the static scattering problem specialized to the case of thin planar dielectric plates is presented, along with an efficient numerical routine. Dipole moments are obtained over a range of permittivities for plates with several thicknesses and a variety of cross-sectional shapes, and the shape dependence is discussed.

42.68.Mj, 77.30. + d

*Now with the Electrical Engineering and Applied Physics Department, Case Western Reserve University, Cleveland, OH 44106.

Introduction

The analysis of the scattering and absorption of electromagnetic radiation by distributions of particles is important in the study of aerosols and their effect on the optical properties of the earth's atmosphere. The effect is usually studied by parameterizing the aerosol in terms of the density of the constituent particles as well as the particle shape,size and composition. Most aerosols contain particles with a variety of shapes and orientations, and it would be difficult, if not impossible, to include the precise features of a particle in any scattering calculation. For this reason and to simplify the computational task, the particles are often modelled using equivalent spheres [1]. The use of spheroids has also been suggested [2], but in order to judge the adequacy of these approximations it is important to know how the geometry and material composition of a particle affect its scattering.

The particles which are studied in this paper are thin plates having length to thickness ratios ranging from 10:1 to 1000:1. Several simple shapes are examined including a circle, square, 2:1 rectangle, equilateral triangle, and a bowtie formed by connecting two equilateral triangles at their vertices. The bowtie, being a reentrant shape, gives results which differ noticably from those for the other (convex) shapes. This is an interesting phenomenon since many aerosols are composed of particles of reentrant shape.

To make possible the analysis of these particles, a stable integral equation formulation for the scattered field is presented along with an efficient numerical implementation. The scattered fields for the various shapes are summarized through the calculation of the electric polarizability tensor elements, and these quantities are displayed over a range of permittivities.

Integral Equations

The problem considered is that of a linearly polarized plane electromagnetic wave incident upon a homogeneous isotropic dielectric non-magnetic plate. The plate is assumed flat with uniform thickness t centered on the z = 0 plane. The incident electric field is taken as

$$\bar{E}^{inc} = \hat{a} \exp(ik\hat{k}\cdot\bar{r}) \tag{1}$$

where $\hat{k}$ and $\hat{a}$ are unit vectors specifying the directions of incidence and the electric field (or polarization) respectively. Mks units are employed and a time factor $e^{-i\omega t}$ is suppressed. Since the permeability of the plate is the same as that of the surrounding free space medium, the total electric field everywhere can be expressed in terms of an electric Hertz vector and written as [3]

$$\bar{E}(\bar{r}) = \bar{E}^{inc}(\bar{r}) + (\varepsilon_r - 1)(\nabla\nabla\cdot + k^2) \int_V \bar{E}(\bar{r}')G(\bar{r}|\bar{r}')dV' \tag{2}$$

where ε_r is the relative permittivity. The integration is over the volume V of the plate and G is the free space Green's function

$$G(\bar{r}|\bar{r}') = \frac{e^{ik|\bar{r}-\bar{r}'|}}{4\pi|\bar{r} - \bar{r}'|} .$$

By allowing $\bar{r}$ to lie in V, (2) becomes a volume integral equation for the interior electric field from which the field everywhere can then be found.

The above formulation is valid for a body of arbitrary shape and any electrical size, and the solution is naturally frequency dependent,

but if the maximum dimension L is small compared to the free space wavelength $2\pi/k$, a low frequency analysis is possible. For sufficiently small kL the fields in the immediate vicinity of the plate are then expanded in power series in k, viz.

$$\bar{E} = \sum_{m=0}^{\infty} (ik)^m \bar{E}_m \quad .$$

The leading (static) term corresponds to Rayleigh scattering, and since, for many purposes, this is sufficient to describe the scattering, attention will be confined to this case. In the near field (2) now reduces to

$$\bar{E}_0(\bar{r}) = \bar{E}_0^{inc}(\bar{r}) + (\epsilon_r - 1)\nabla\nabla\cdot \int_V \bar{E}_0(\bar{r})G_0(\bar{r}|\bar{r}')dV' \qquad (3)$$

where

$$G_0(\bar{r}|\bar{r}') = \{4\pi|\bar{r} - \bar{r}'|\}^{-1} \quad ,$$

and because $\nabla \times \bar{E}_0 = 0$, $\bar{E}_0$ can be expressed in terms of a static potential ϕ as

$$\bar{E}_0 = -\nabla\phi \quad .$$

The corresponding incident field potential is $-\hat{a}\cdot\bar{r}$, which leads us to write

$$\phi = \sum_{i=1}^{3} \hat{a}\cdot\hat{x}_i\phi_i$$

where the x_i, $i = 1,2,3$ with $x_3 = z$ are Cartesian coordinates. Thus, the general problem can be solved by considering separately the three incident

field potentials $-x_i$ with $i = 1,2,3$, and a volume integral equation from which to obtain ϕ_i is then

$$\phi_i(\bar{r}) = -x_i - (\varepsilon_r - 1) \int_V \nabla'\phi_i(\bar{r}') \cdot \nabla' G_0(\bar{r}|\bar{r}')dV' \quad . \quad (4)$$

The resulting expression for the scattered electric field in the far zone ($kr \to \infty$) of the plate is [4]

$$\bar{E}^s(\bar{r}) = -k^2 \frac{e^{ikr}}{4\pi\varepsilon_0 r} \hat{r} \times (\hat{r} \times \bar{p}) \quad (5)$$

where ε_0 is the permittivity of free space. The field is attributable to an electric dipole whose moment $\bar{p}$ can be written as [5]

$$\bar{p} = \varepsilon_0 \bar{\bar{P}} \cdot \hat{a} \quad (6)$$

where $\bar{\bar{P}}$ is the electric polarizability tensor. The elements P_{ij} are expressible as weighted surface integrals of the electrostatic potentials:

$$P_{ij} = -(\varepsilon_r - 1) \int_B \hat{n} \cdot \hat{x}_i \phi_j \, dS$$

where $\hat{n}$ is the outward unit normal to the surface B of the plate. The tensor is a function only of the geometry and permittivity, and for real ε_r the tensor is real and symmetric, with at most six independent elements. From (5) the total scattering and extinction cross sections are

$$\sigma_T = \frac{k^4}{6\pi} \hat{a} \cdot (\bar{\bar{P}} \cdot \bar{\bar{P}}^*) \cdot \hat{a} \quad (7)$$

and

$$\sigma_E = k \, \mathrm{Im} \, \hat{a} \cdot \bar{\bar{P}} \cdot \hat{a} \tag{8}$$

respectively, where the asterisk denotes the complex conjugate.

In practice a volume integral equation such as (4) is not usually convenient for numerical purposes, and it is customary (see, for example, [6]) to convert it to a surface integral equation. The resulting equation is still exact and has been employed to treat the problem of low frequency scattering by rotationally symmetric particles [4,7] and rectangular parallelepipeds [8]. In the particular case when the length to width ratio is small, these bodies reduce to circular and rectangular plates respectively. An alternative approach is to invoke the thinness property of a plate at the outset by expanding the potential ϕ_i in powers of z ($=x_3$). From symmetry considerations the dominant term for $|z| \leq t/2 << L$ is the zeroth order one if i = 1 or 2 and the first order one if i = 3, and by assuming this dependence over the entire region occupied by the plate, the volume integral in (4) can be reduced [9] to an integral over (say) the upper surface z = t/2 of the plate. For the potentials ϕ_1 and ϕ_2 the integral equation becomes

$$\phi_i(\bar{r}) = -x_i - (\varepsilon_r - 1) \int_S \nabla'_S \phi_i \cdot \nabla'_S G_1 \, dS' \tag{9}$$

with

$$G_1 = \int_{-t/2}^{t/2} G_0 \, dz' \, , \tag{10}$$

whereas for ϕ_3

$$\phi_3(\bar{r}) = -t - \frac{2}{t} (\varepsilon_r - 1) \int_S \phi_3 G_2 \, dS' \tag{11}$$

with

$$G_2 = G_0 \Big|_{z'=-t/2}^{z'=t/2} \tag{12}$$

for $\bar{r}$ on S where S is the upper surface z = t/2 of the plate.

The above equations can be simplified by allowing t to approach zero with $t(\varepsilon_r - 1)$ held constant. Equation (9) then becomes

$$\phi_i(\bar{r}) = -x_i - t(\varepsilon_r - 1) \int_S \nabla'_s \phi_i \cdot \nabla'_s G_0 \, dS' \tag{13}$$

for z, z' = 0, and this is identical to the low frequency limit of the integral equation for a resistive plate in the plane z = 0. Although a resistive sheet is often used as an approximation to a thin dielectric layer [10], its justification requires that Im $\varepsilon_r \gg 1$, and since the polarization current is confined to the plane of the sheet, the normal component of the induced electric dipole moment is zero. The present formulation is not limited in this manner, and because of this, (9) and (11) should provide a more accurate approximation for any plate thickness $t \ll L$ and any permittivity, real as well as complex.

Method of Solution

Equations (9) and (11) provide an approximation to the problem of the static scattering from a thin plate. The numerical solution of these equations may be obtained by discretizing the problem using the finite element method [11]. The plate, or more specifically the surface S, is divided into triangular elements on which a set of linear basis functions are defined. Pulse basis functions, which are constant over the individual elements, are a popular choice since they simplify the evaluation of the integrals over the subdomains, but are unnecessary in the present case since the contributions of the subdomains can be

evaluated analytically. The basis functions are used to construct a ϕ_i which satisfies (9) or (11), and since the global behavior of ϕ_i, particularly ϕ_1 and ϕ_2, is approximately linear, the linear basis functions permit an accurate solution with a relatively small number of elements. Linear basis functions are also superior to pulse basis functions in that they guarantee C_0 continuity of the solution, which cannot be surpassed even through the use of higher order basis functions.

As an example of the discretization, a 16-sided approximation to a circular plate is shown in Fig. 1. The t's denote the different triangular subdomains, while the p's denote the points which delimit the triangle. The construction of linear basis functions over triangular elements is most naturally accomplished using area coordinates [11]. Given a triangle with vertices $\bar{r}_1 = (x_1,y_1)$, $\bar{r}_2 = (x_2,y_2)$ and $\bar{r}_3 = (x_3,y_3)$, and assuming $\bar{r} = (x,y)$ lies inside the triangle, the area coordinates are defined as

$$L_1 = \frac{\text{area}(\bar{r},\bar{r}_2,\bar{r}_3)}{\text{area}(\bar{r}_1,\bar{r}_2,\bar{r}_3)} \quad , \quad L_2 = \frac{\text{area}(\bar{r}_1,\bar{r},\bar{r}_3)}{\text{area}(\bar{r}_1,\bar{r}_2,\bar{r}_3)}$$

and

$$L_3 = \frac{\text{area}(\bar{r}_1,\bar{r}_2,\bar{r})}{\text{area}(\bar{r}_1,\bar{r}_2,\bar{r}_3)}$$

where $\text{area}(\bar{r}_1,\bar{r}_2,\bar{r}_3)$ is the area of the triangle delimited by the points $\bar{r}_1$, $\bar{r}_2$, and $\bar{r}_3$. The formulation may be restated using determinants as

$$L_1 = \begin{vmatrix} 1 & x & y \\ 1 & x_2 & y_2 \\ 1 & x_3 & y_3 \end{vmatrix} \div \begin{vmatrix} 1 & x_1 & y_1 \\ 1 & x_2 & x_2 \\ 1 & x_3 & y_3 \end{vmatrix}$$

with the L_1 and L_2 defined similarly. The advantage of this notation is that it permits the natural expression of the potential within the triangle in terms of the potentials at the vertices. Using the above definitions, $f(x,y) = L_1$ has values $f(x_1,y_1) = 1$ and $f(x_2,y_2) = f(x_3,y_3) = 0$. Thus, if the potential ϕ_i is known as $\phi_i(x_1,y_1) = \Phi_1$, $\phi_i(x_2,y_2) = \Phi_2$ and $\phi_i(x_3,y_3) = \Phi_3$, then inside the triangle

$$\phi_i(x,y) = \Phi_1 L_1 + \Phi_2 L_2 + \Phi_3 L_3$$

and

$$\nabla_S \phi_i(x,y) = \Phi_1 \bar{u}_1 + \Phi_2 \bar{u}_2 + \Phi_3 \bar{u}_3$$

where the $\bar{u}_i$ are the (constant) surface gradients of the L_j, $j = 1,2,3$.

Assuming a discretization similar to that in Fig. 1, let the total number of points needed to delimit the discretization be N with the points labeled p_j, $j = 0,1,2,\ldots,N-1$. Assuming that each point p_j is contiguous with M_j elements, (9) becomes

$$\phi_i = -x_i - (\varepsilon_r - 1) \sum_{j=0}^{N-1} \Phi_j \sum_{m=0}^{M_j-1} \int_{S_{jm}} \bar{u}_{jm} \cdot \nabla_S' G_1 \, dS' \tag{14}$$

where S_{jm} denotes the mth triangular element associated with the point p_j, and $\bar{u}_{jm}$ denotes a vector $\bar{u}$ as defined above associated with the region S_{jm} and the point p_j. Equation (14) may be converted to a system of N linear equations in N unknowns by writing

$$\Phi_k = -x_i - (\varepsilon_r - 1) \sum_{j=0}^{N-1} \Phi_j \sum_{m=0}^{M_j-1} \int_{S_{jm}} \bar{u}_{jm} \cdot \nabla_S' G_{1k} \, dS'$$

where G_{1k} denotes G_1 with the field point at p_k, i.e., $G_{1k} = G_1|_{\bar{r}=\bar{r}_{pk}}$. This may be recast as the matrix problem

$$X = (A - I)\Phi \quad ,$$

where I is the identity matrix,

$$\Phi = [\Phi_0, \Phi_1, \ldots, \Phi_{N-1}]^T$$

$$X = [\hat{x}_i \cdot \bar{r}_{p_0}, \hat{x}_i \cdot \bar{r}_{p_1}, \ldots, \hat{x}_i \cdot \bar{r}_{p_{N-1}}]^T$$

and A is a matrix whose elements a_{kj} are given by

$$a_{kj} = -(\varepsilon_r - 1) \sum_{m=0}^{M_j - 1} \int_{S_{jm}} \bar{u}_{jm} \cdot \nabla'_s G_{1k} \, dS' \quad . \quad (15)$$

The q_{kj} can be evaluated by decomposition into several integrals of the form

$$\int_{S_{jm}} \frac{\partial G_{1k}}{\partial x_\ell} \, dS' \qquad (\ell = 1,2) \quad .$$

As an example of how the evaluation proceeds, let the field point be p_0 and the triangular element be t_{10} as shown in Fig. 1. Choosing $\ell = 1$ gives

$$I_1 \equiv \int_{t_{10}} \frac{\partial G_{1,0}}{\partial x'} \, dS' = \int_0^1 dy' \int_{1.5(1+y')}^{3} dx' \frac{\partial G_{1,0}}{\partial x'} \, dS'$$

$$= \int_0^1 dy' \, G_{1,0}\Big|_{1.5(1+y')}^{3} \quad .$$

Since the field point is p_o, it follows that $x = y = 0$ and $z = t/2$. Letting $\eta' = t/2 - z'$ and changing the order of integration yields

$$I_1 = \frac{1}{4\pi} \int_0^t d\eta' \int_0^1 dy' \, [x'^2 + y'^2 + z'^2]^{-1/2} \Big|_{x'=3/2(1+y')}^{x'=3} . \tag{16}$$

This is the basic type of integral encountered in evaluating the a_{kj}, but the integrand becomes more complicated as the field point is moved from the origin and the element S_{jm} changes orientation and shape. In each instance, however, (16) can be converted [12, §2.261] to a number of integrals of the form

$$\int_0^t \ln[a(b + \eta^2)^{-1/2} + c] \, d\eta \quad ,$$

which can be evaluated using integration by parts in conjunction with [12, §2.267.1]. Although the analytic evaluation of the matrix elements in (15) is cumbersome, the resulting algorithm is both faster and more accurate than one which relies on numerical integration.

The evaluation of (11) for the potential ϕ_3 associated with the normal excitation is accomplished in a manner similar to the above. Simplifications result since the derivatives of ϕ_3 are not involved and the reduction [13] to a line integrand can be profitably employed.

After the potential has been computed there remains the problem of calculating the tensor elements P_{ij}. If the plate has an axis of symmetry in addition to the z axis the polarizability tensor $\bar{\bar{P}}$ is diagonal, and the P_{ii} are given by

$$P_{ii} = -t(\varepsilon_r - 1) \int_C \hat{n} \cdot \hat{x}_i \phi_i \, d\ell' \qquad (i = 1,2) \tag{17}$$

$$P_{33} = -2(\varepsilon_r - 1)\int_S \phi_3 \, dS \quad . \tag{18}$$

where C is the edge of the particle.

For particles which are very thin and/or have ε_r close to unity, the potential inside and on the particle may be approximated by assuming that the scattered field is small compared to the incident field. Writing

$$\phi_i = -x_i + \phi_i^S \qquad (i = 1,2)$$

and assuming that $|\nabla x_i| >> |\nabla \phi_i^S|$, the divergence theorem yields

$$P_{ii} = -(\varepsilon_r - 1)\hat{x}_i \cdot \int_V \{-\nabla x_i + \nabla \phi_i^S\} \, dV \cong (\varepsilon_r - 1)V \tag{19}$$

(i = 1,2) where V is the volume of the particle. Similarly, for the normal excitation

$$\phi_3 = \frac{1}{\varepsilon_r}(-z + \phi_3^S)$$

inside and on the plate, and then

$$P_{33} = -(\varepsilon_r - 1)\hat{z} \cdot \int_V \frac{1}{\varepsilon_r}\{-\nabla z + \nabla \phi_3^S\} \, dV \cong \frac{1}{\varepsilon_r}(\varepsilon_r - 1)V \ , \tag{20}$$

Numerical Results

When considering scattering from small thin particles it is often convenient to approximate the scattered field using the small scattered field approximation given in the previous section. The validity of this approximation generally depends upon such gross parameters of the particle as the volume, thickness and permittivity. In Fig. 2 the dipole moment per unit volume resulting from the electric field in the plane of the plate is shown for several thin circular disks. The data were obtained using a program based on the algorithm described above with the circular plate being defined by a 36-sided approximation consisting of 348 triangular elements. The maximum error here and in the following graphs is believed less than a few percent. Consistent with physical expectation, the calculated dipole moments are almost those for the limiting spheroid when the thickness/diameter and permittivity are small. For large values of permittivity, P_{11}/V must eventually converge to the perfectly conducting limit, and this is evinced by the thicker disks.

The data is Fig. 3 have been normalized to show the region in which the resistive sheet approximation (see (13)) is valid. The functional dependence of the resistive sheet approximation is upon the product $(\varepsilon_r - 1)t$, with no dependence on $(\varepsilon_r - 1)$ or t individually. In Fig. 3 $(\varepsilon_r - 1)t$ was held constant at each of three values while t/d was swept from 0.001 to 0.1. The sheet approximation appears quite justified for $(\varepsilon_r - 1)t/d = 0.1$, but degenerates for larger values, i.e., for thicker plates or higher permittivities. The normalization of P_{11}/V by t/d is used to provide a P_{11} which is normalized by a volume parameter not dependent on the thickness of the plate.

The quantity P_{33}/V is shown for various plate thicknesses and permittivities in Fig. 4. Again, the disk model is an accurate predictor of P_{33}/V for small values of thickness/diameter and $\varepsilon_r - 1$. The almost exact match of the t/d = 0.001 plate with the limiting spheroid belies a rather curious behavior of the potential on the surface of the plate. Since the plate thickness is uniform, the potential on the surface of the plate is not (c.f., a thin plate spheroid), and within a ring of depth t near the edge of the plate the potential varies quite rapidly. This is entirely consistent with the physics of the problem, but it makes modelling the solution quite difficult. The quantity P_{11}/V does not reflect this peculiar behavior since P_{11} is calculated from an integral of the potential and the rise in the potential occurs over a very small region.

Figures 5 and 6 compare data for the circular disk having t/d = 0.1 to values for other shapes with the same thickness and volume as the disk. The various shapes produes dipole moments which are almost identical for small values of ε_r, but diverge as $\varepsilon_r \to \infty$. Shapes which have length to width ratios comparable to unity produce dipole moments which are similar over a wide range of ε_r, but the rectangle and bowtie have relatively large dipole moments when the electric field is parallel to the long axis of the plate. As shown in [9], a knowledge of the length, width, thickness, and permittivity are generally sufficient to provide a good estimate of the dipole moment for convex plates. For non-convex shapes such estimates are invalid, as evidenced by the bowtie which behaves differently from the convex shapes at high permittivities. For thinner plates the dipole moments of the triangle, square, rectangle, and bowtie converge to the oblate spheroid results at about the same rate as the circular disk values. When the

incident electric vector is in the plane of the plate, making the plate thinner causes the shape effects to appear at higher values of the permittivity, but with normal excitation the shape has virtually no effect if the plate is thin.

Conclusions

The data presented in this paper were obtained using an integral equation formulation which was specialized to the case of a thin plate. The discretization of the problem in conjunction with a piecewise linear expansion of the potential in the plane of the plate makes possible the analytic evaluation of the integrals over the subdomains. This particular formulation of the problem provides accurate results for a relatively small amount of computation time. The zero thickness oblate spheroid has been shown to be a useful model, particularly for very thin plates with small permittivities. The shape of the particle becomes important when either the thickness of the plate or the permittivity is increased and this is the region where the program is most valuable.

In distributions of particles the excitation of the individual particles may be random. This randomization may be accounted for by aspect averaging the dipole moments associated with the particular shape, and though this reduces the effect of shape on the dipole moments for most of the particles examined, the bowtie still appears different from the other geometries. The bowtie was the only reentrant shape examined, and if this behavior applies to other reentrant shapes, it could make questionable the use of simple convex models for these plates.

All of the data presented were obtained for relative permittivities which are purely real and greater than unity. In fact, the program is capable of analyzing plates with arbitrary complex permittivities and this is an area of intended future investigation. Preliminary results indicate that when the real part of the permittivity is negative, the similarity of the dipole moments for particles of different shape no longer holds, and particularly in the vicinity of resonances [2], the results are highly shape dependent.

Acknowledgement

This research was supported by the U.S. Army Chemical Systems Laboratory under Contract No. DAAK11-82-K-0007.

References

1. A. C. Holland, G. Gagne, Appl. Opt. 9, 1113-1121 (1970).
2. T.B.A. senior. H. Weil, Appl. Phys. B 29, 117-124 (1982).
3. D. S. Jones, Methods in Electromagnetic Wave Propagation (Clarendon Press, Oxford 1979).
4. T.B.A. Senior, Radio Sci. 11, 477-482 (1976).
5. J. B. Keller, R. E. Kleinman, T.B.A. Senior, J. Inst. Maths Applics 9, 14-22 (1972).
6. D. S. Jones, Q. J. Mech. Appl. Math. 33, 105-122 (1980).
7. T.B.A. Senior, T. M. Willis III, IEEE Trans. AP-30, 1271 (1982).
8. D. F. Herrick, T.B.A. Senior, Appl. Phys. 13, 175-183 (1977).
9. D. A. Ksienski, Scattering by Distribitions of Small Thin Particles, Ph.D. Dissertation (The University of Michigan, Ann Arbor, MI 1984).
10. R. F. Harrington, J. R. Mautz, IEEE Trans. AP-23, 531-534 (1975).
11. O. C. Zienkowicz. The Finite Element Method (McGraw Hill, London 1982).
12. I. E. Gradshteyn, I. M. Ryzhik, Table of Integrals, Series, and Products (Academic Press, New York 1980).
13. D. R. Wilton, S. M. Rao, A. W. Glisson, D. H. Schaubert, O. M. Al-Bundak, C. M. Butler, IEEE Trans. AP-32, 276-281 (1984).

Legends for Figures

Fig. 1: Typical element definition for an approximation to a circular plate. Only a quarter of the plate is shown, and a much finer mesh was used in all of the calculations.

Fig. 2: P_{11}/V for circular plates whose thickness/diameter is (a) 0.1, (b) 0.01 and (c) 0.001, and for a zero thickness oblate spheroid (d).

Fig. 3: $P_{11}t/(Vd)$ for a circular plate with $(\varepsilon_r - 1)t/d$ held constant at (a) 10, (b) 1 and (c) 0.1.

Fig. 4: P_{33}/V for circular plates with thickness/diameter equal to (a) 0.1, (b) 0.01 and (c) 0.001. The values for a zero thickness oblate spheroid are almost identical to those for the thinnest plate.

Fig. 5: Comparison of P_{11}/V (——) and P_{22}/V (---) for (a) a circular plate, (b) a square, (c) an equilateral triangle, (c) a 2:1 rectangle and (e) a bowtie. All the plates have thickness/diameter = 0.1 and the same volume, and in the case of the rectangle and bowtie the x_2 axis is the longer symmetry axis.

Fig. 6: Comparison of P_{33}/V for (a) a circular plate, (b) a square, (c) an equilateral triangle, (d) a 2:1 rectangle and (c) a bowtie. All the plates have thickness/diameter = 0.1 and the same volume.

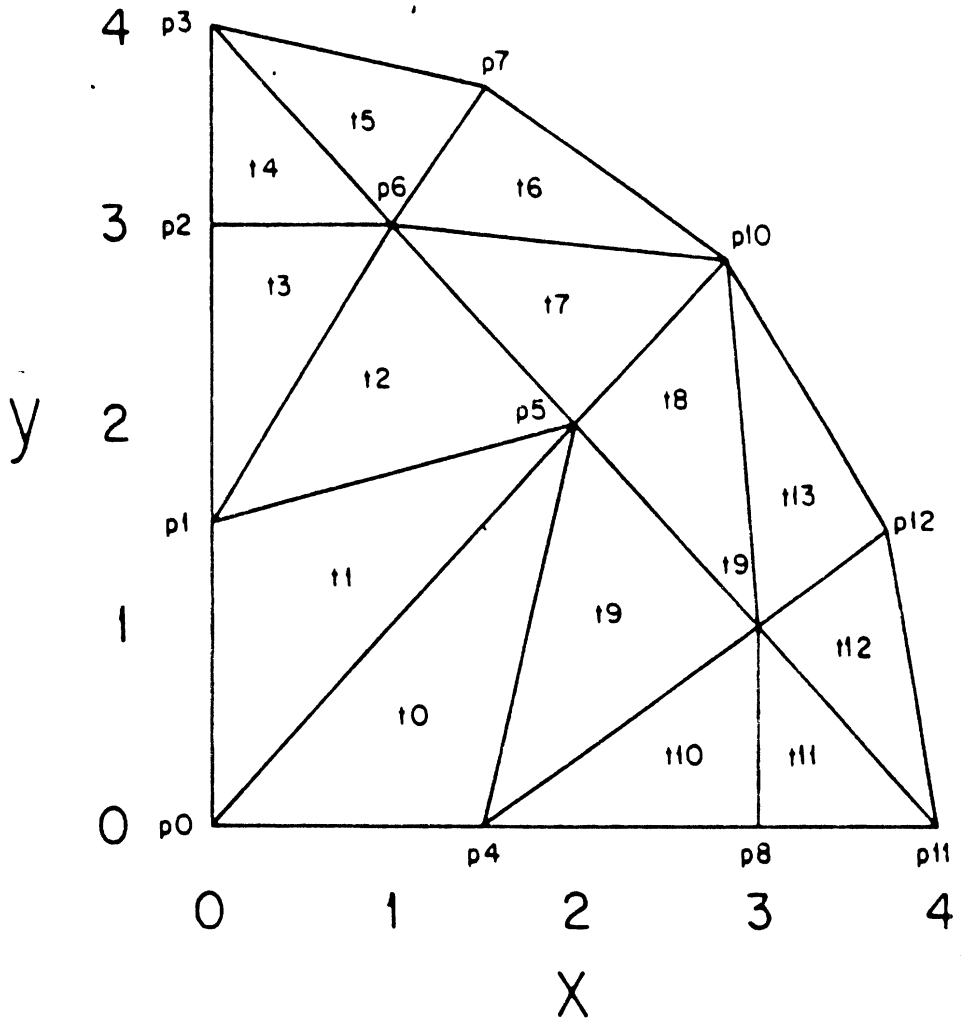

Fig. 1: Typical element definition for an approximation to a circular plate. Only a quarter of the plate is shown, and a much finer mesh was used in all of the calculations.

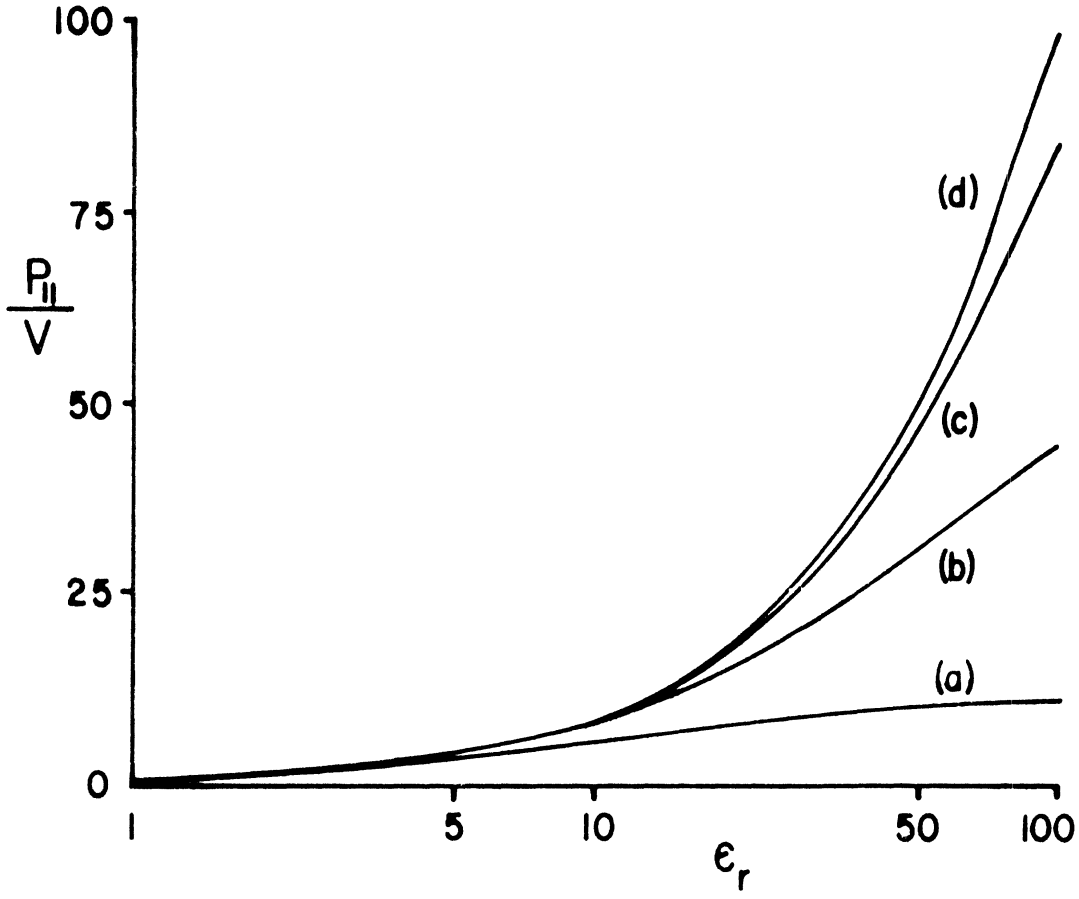

Fig. 2: P_{11}/V for circular plates whose thickness/diameter is (a) 0.1, (b) 0.01 and (c) 0.001, and for a zero thickness oblate spheroid (d).

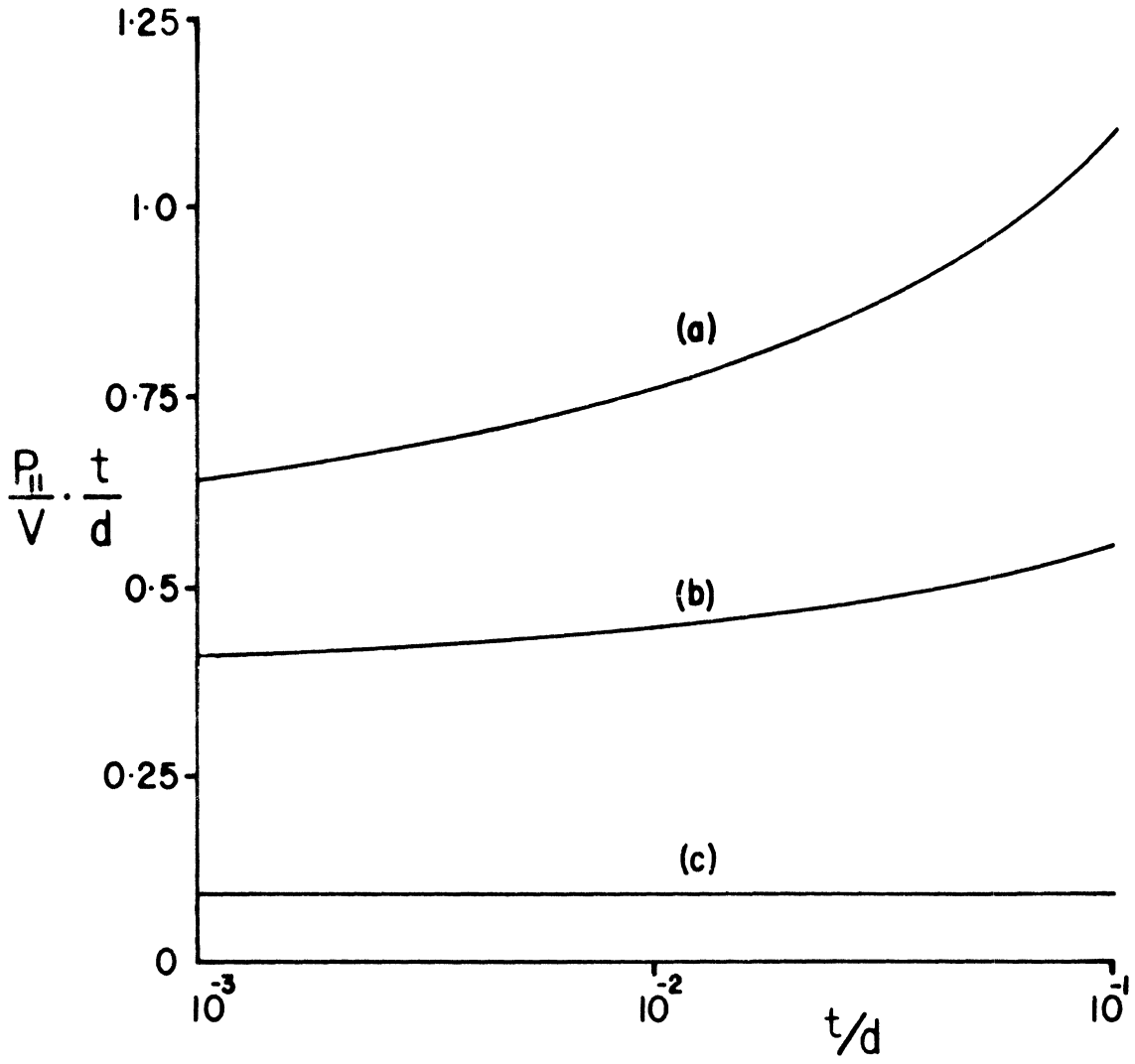

Fig. 3: P_{11} t/(Vd) for a circular plate with $(\varepsilon_r - 1)t/d$ held constant at (a) 10, (b) 1 and (c) 0.1.

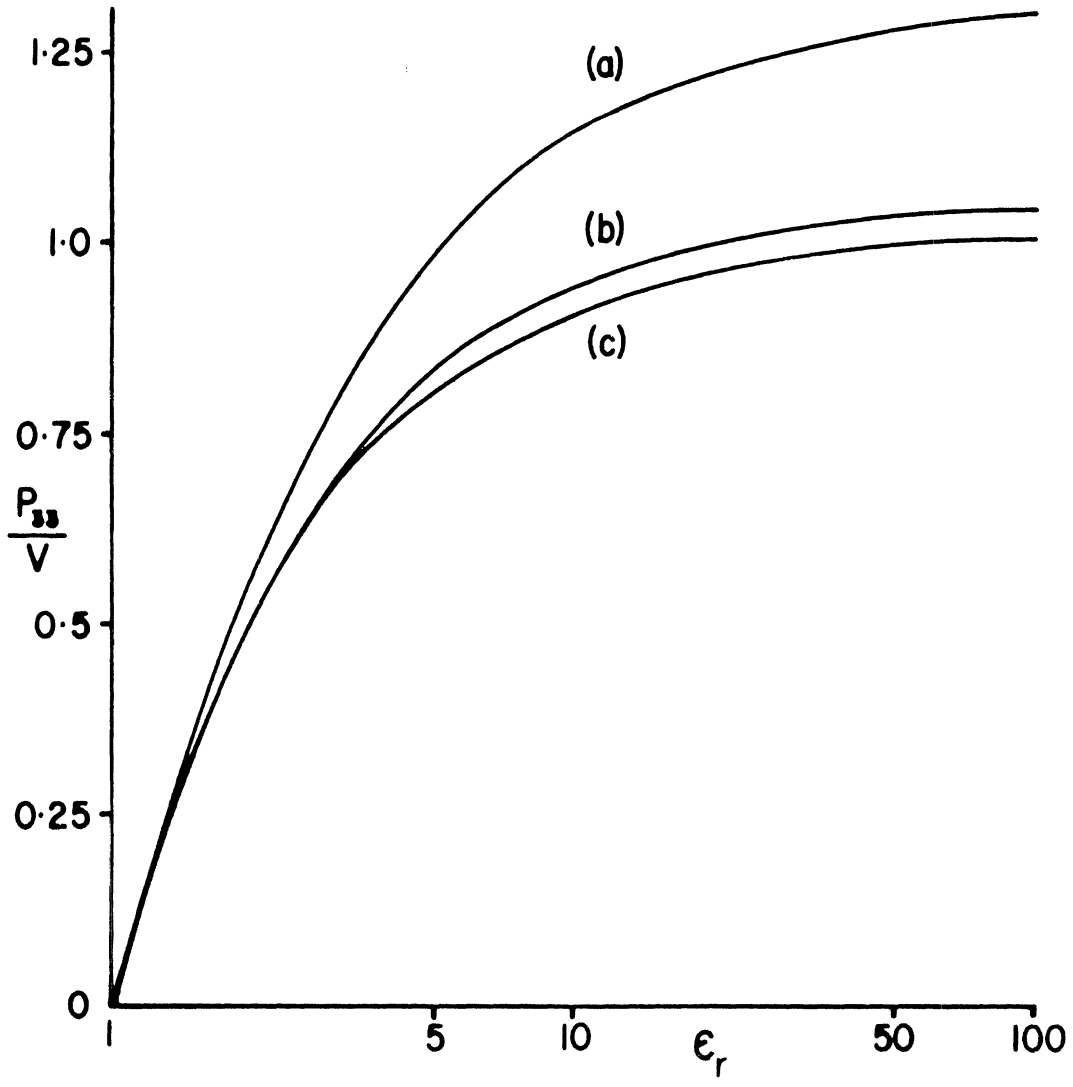

Fig. 4: P_{33}/V for circular plates with thickness/diameter equal to (a) 0.1, (b) 0.01 and (c) 0.001. The values for a zero thickness oblate spheroid are almost identical to those for the thinnest plate.

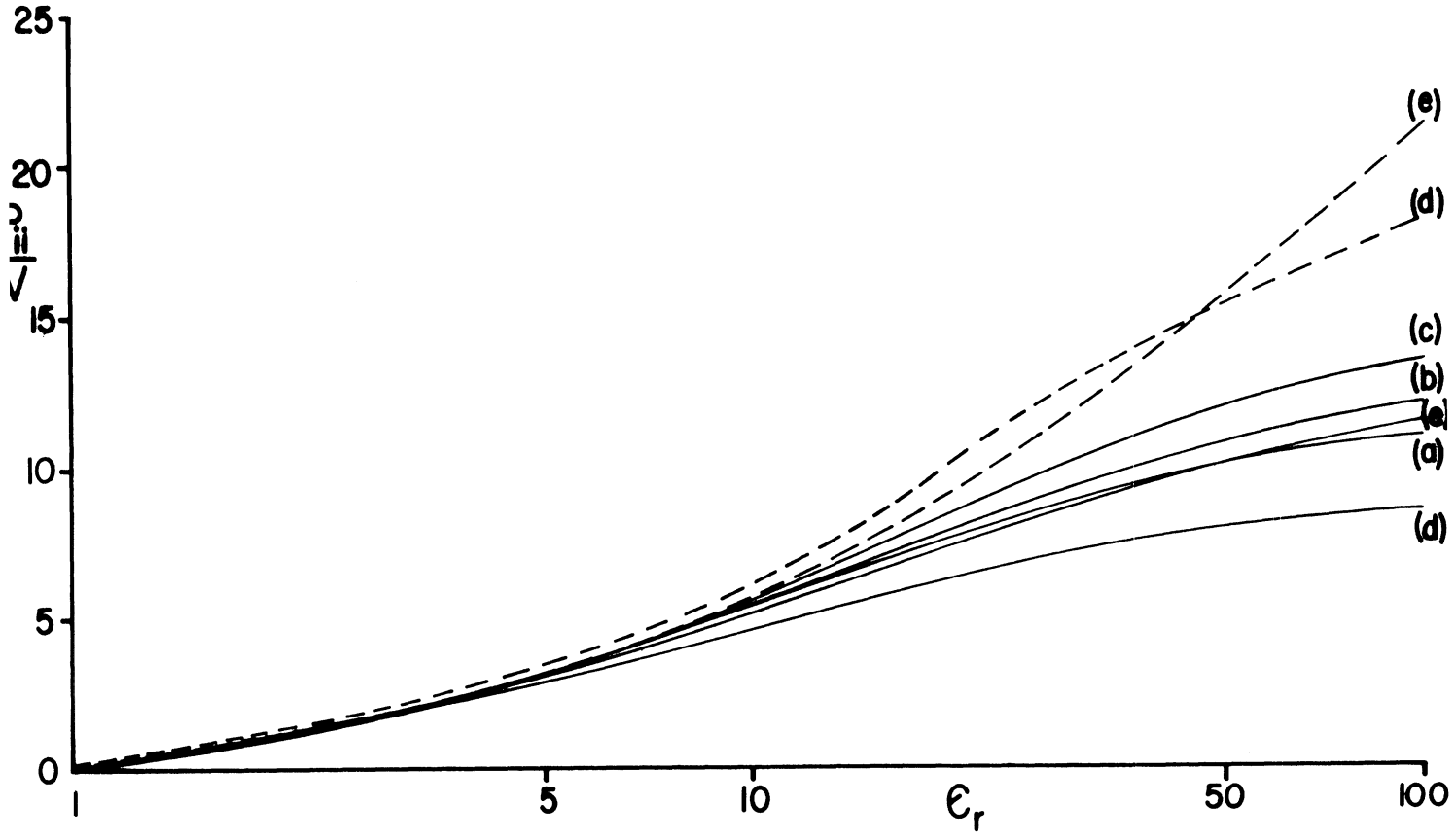

Fig. 5: Comparison of P_{11}/V (——) and P_{22}/V (---) for (a) a circular plate, (b) a square, (c) an equilateral triangle, (c) a 2:1 rectangle and (e) a bowtie. All the plates have thickness/diameter = 0.1 and the same volume, and in the case of the rectangle and bowtie the x_2 axis is the longer symmetry axis.

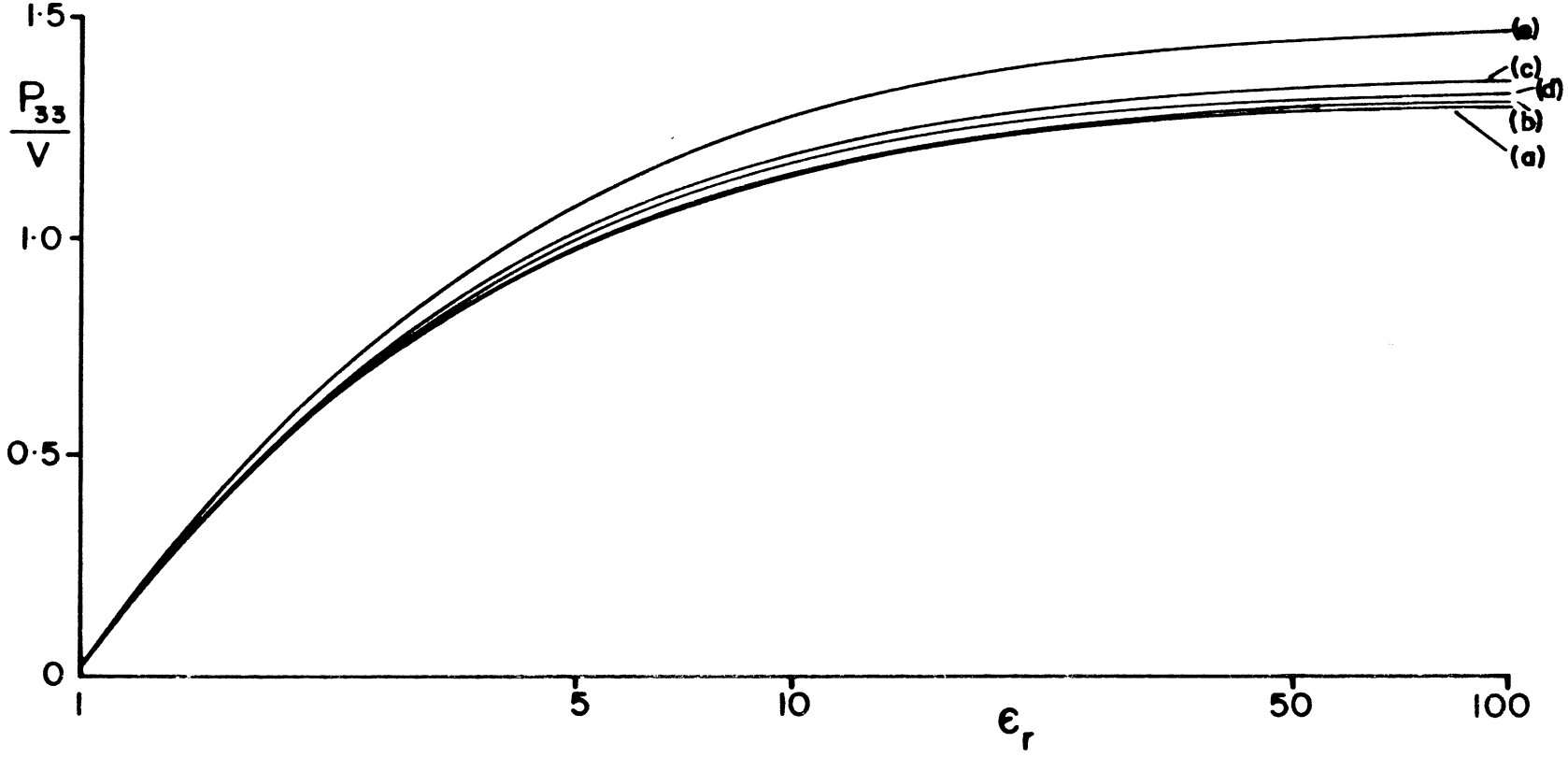

Fig. 6: Comparison of P_{33}/V for (a) a circular plate, (b) a square, (c) an equilateral triangle, (d) a 2:1 rectangle and (c) a bowtie. All the plates have thickness/diameter = 0.1 and the same volume.

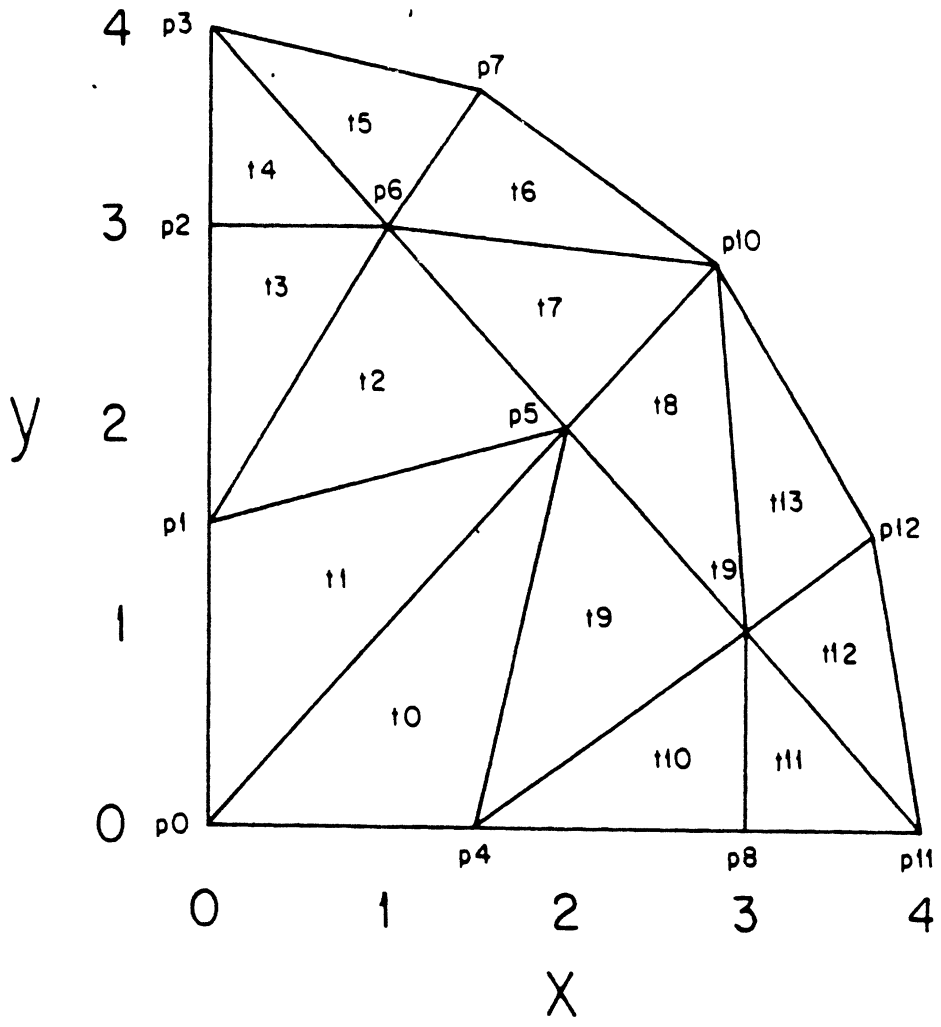
4
3
2
1
0
y
p3
p7
p6
p2
p10
p5
p1
p12
p0
p4
p8
p11
t0
t1
t2
t3
t4
t5
t6
t7
t8
t9
t9
t10
t11
t12
t13
0
1
2
3
4
X

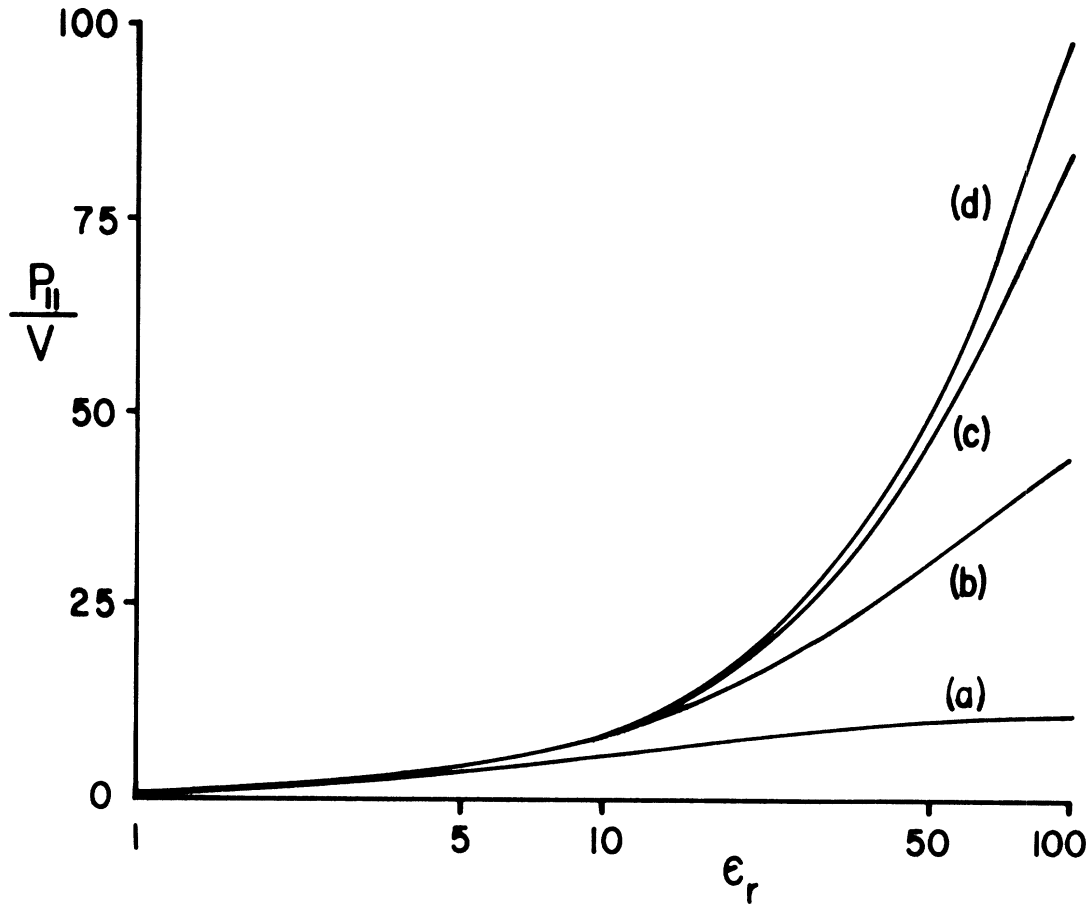
100
75
50
25
0
$\frac{P_{11}}{V}$
(d)
(c)
(b)
(a)
1
5
10
50
100
ϵ_r

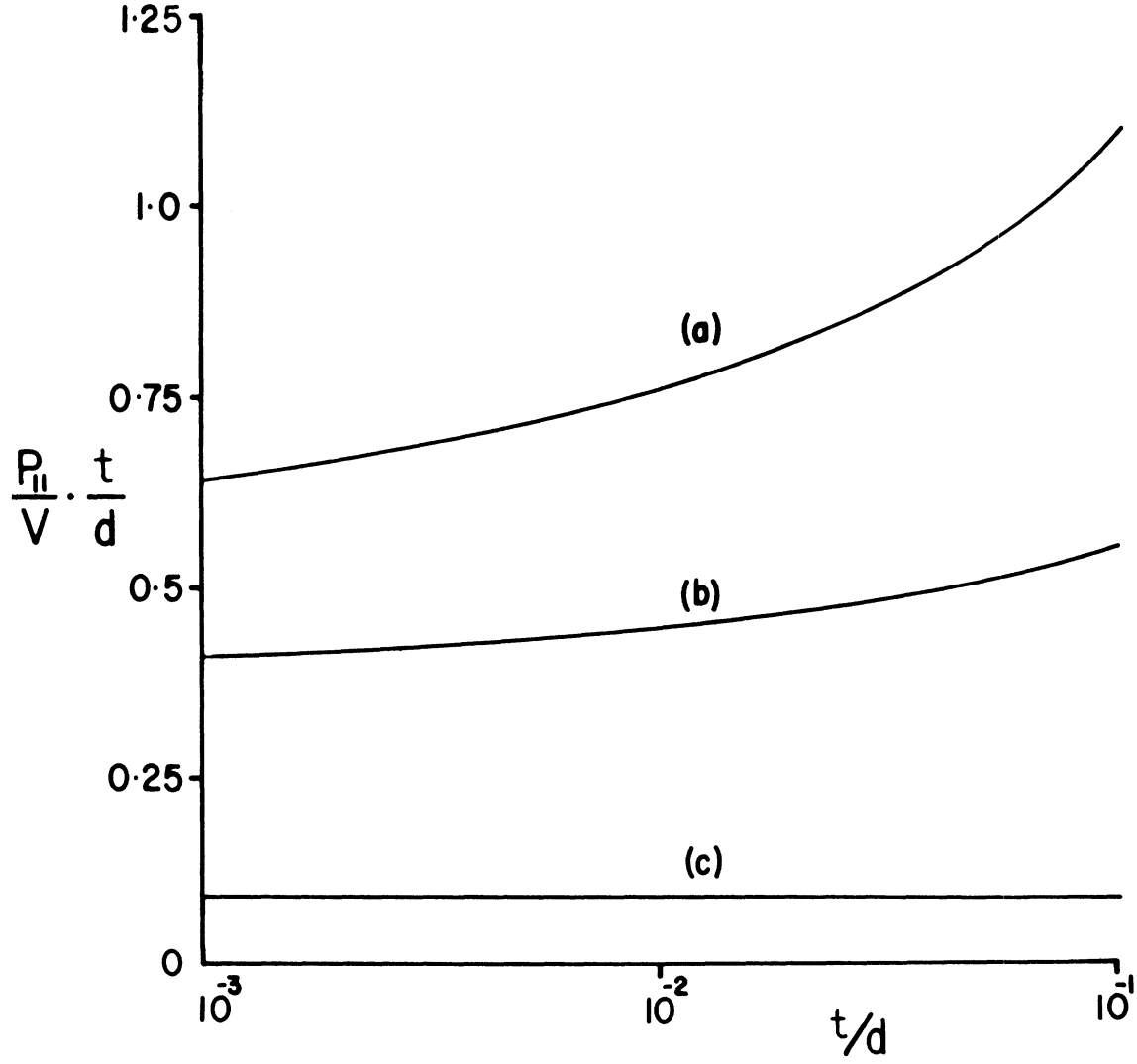
1·25
1·0
0·75
0·5
0·25
0
$\frac{P_{11}}{V} \cdot \frac{t}{d}$
(a)
(b)
(c)
10^{-3}
10^{-2}
10^{-1}
t/d

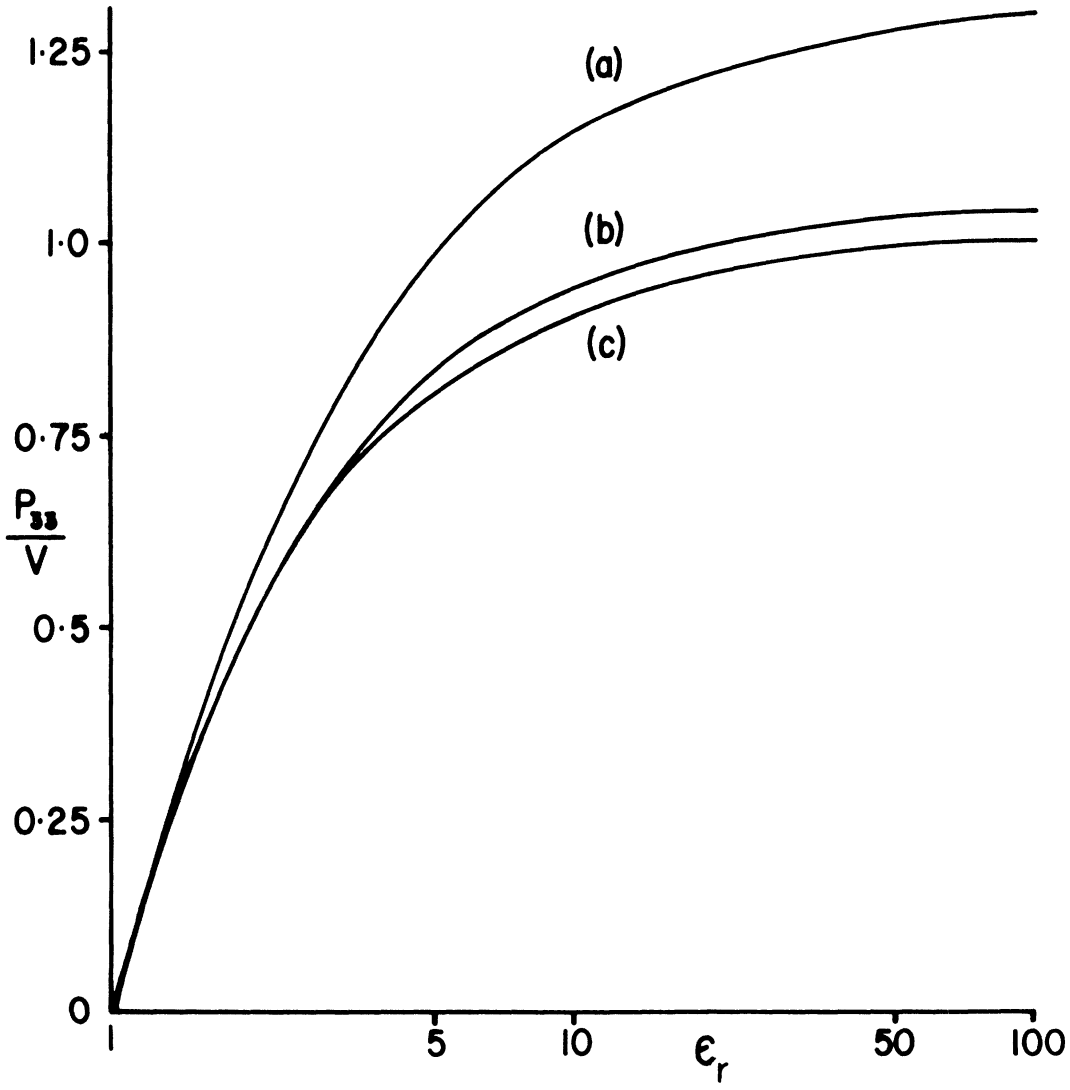
1·25
1·0
0·75
$\frac{P_{33}}{V}$
0·5
0·25
0
1
5
10
50
100
ϵ_r
(a)
(b)
(c)

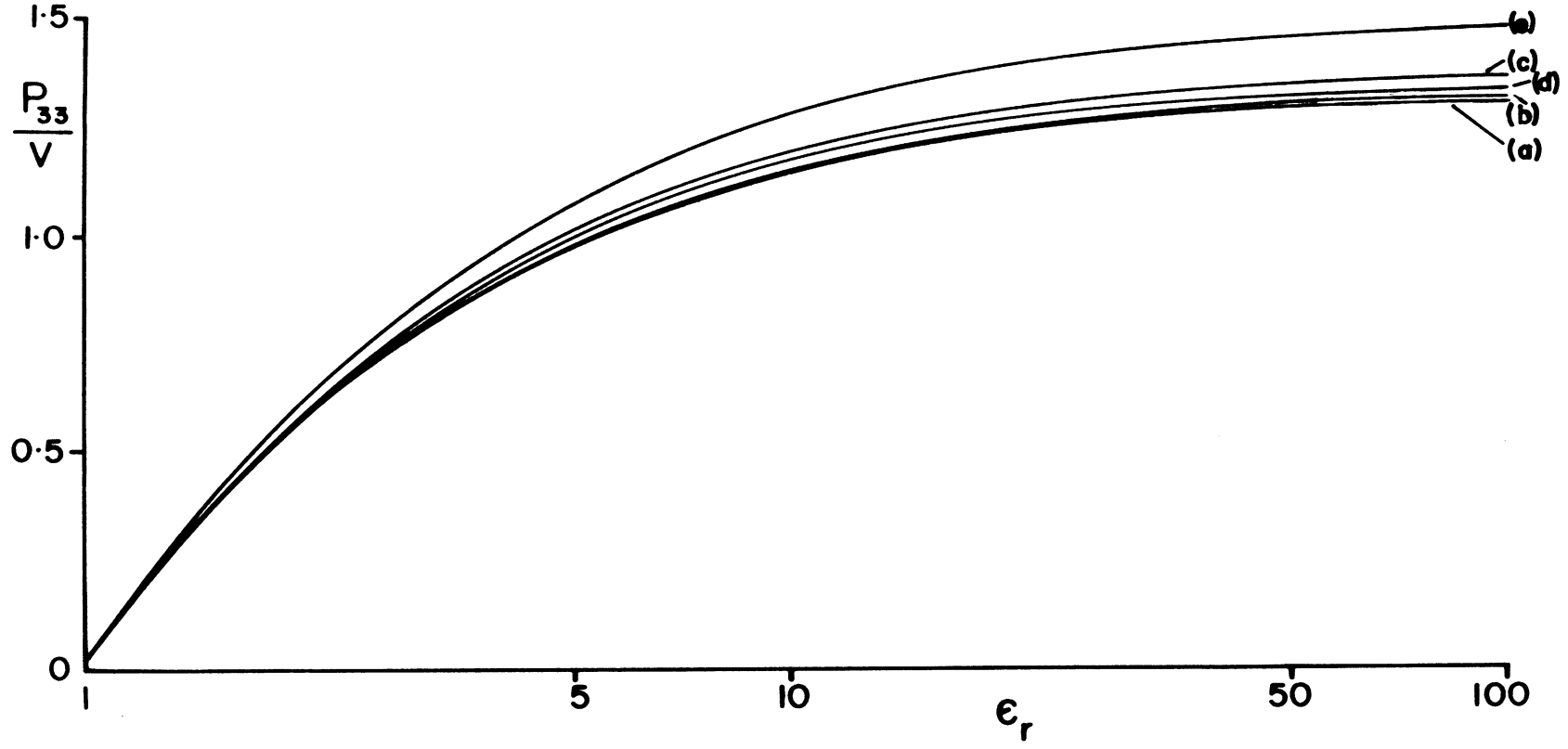
1·5
$\frac{P_{33}}{V}$
1·0
0·5
0
1
5
10
50
100
ϵ_r
(a)
(c)
(d)
(b)
(a)